

International Journal of Nanoelectronics and Materials

IJNeaM -

ISSN 1985-5761 | E-ISSN 2232-1535



Simulation and analysis of film bulk acoustic wave resonator for gas sensor

Nurul Izza Mohd Nor a,b *, Muhammad Rosmaidie Roslan a, Nazuhusna Khalid a,b, Hasnizah Aris a,b, Muhammad Mahyiddin Ramli a,b,c, and Mohd Syafiq Mispan d

^aFaculty of Electronic Engineering & Technology, Universiti Malaysia Perlis, Arau, Perlis, Malaysia

^bCentre of Excellence for Micro System Technology (MiCTEC), Universiti Malaysia Perlis, Arau, Perlis, Malaysia

^cInstitute of Nano Electronic Engineering, Universiti Malaysia Perlis, Kangar, Perlis, Malaysia

^aFaculty of Electrical and Electronic Engineering Technology, Universiti Teknikal Malaysia, Melaka, Malaysia

* Corresponding author. E-mail: izza@unimap.edu.my

Received 16 December 2024, Revised 11 September 2025, Accepted 03 October 2025

ABSTRACT

Developing gas sensors using Film Bulk Acoustic Resonators (FBARs) presents a multifaceted challenge centred around the identification of optimal piezoelectric and electrode materials. The resonance frequency, a critical parameter, must be precisely controlled to ensure efficient vibration, especially in the presence of specific gases that may alter this frequency. Balancing the quality (Q) factor is essential, as a higher Q factor contributes to sharper resonances, enhancing sensitivity. Hence, this work presents the analysis of various design parameters, piezoelectric materials, and electrode materials in enhancing the Q factor, thus improving the performance of FBAR for gas sensors. Comprehensive one-dimensional (1-D) modelling is utilized to optimize the device performance, focusing on variation of parameters such as thickness, width, and length of each layer of FBAR, piezoelectric materials, aluminium nitride (AlN), zinc oxide (ZnO), and electrode material, aluminium (Al). The optimized FBAR using AlN as the piezoelectric material shows better characteristics compared to FBAR using ZnO. The highest Q factor achieved was 8569 at 1 GHz with the area of 30 μ m.

Keywords: FBAR, Gas sensing, Simulation, AlN, ZnO, Q factor

1. INTRODUCTION

In recent years, concerns about poor air quality are significant because of its direct and indirect harmful effects on individuals' health. Air pollutants, including particulate matter (PM_{2.5} & PM10), toxic gases such as carbon monoxide (CO), hydrogen sulfide (H₂S), nitrogen oxides (NO_X) and sulphur dioxide (SO_X), volatile organic compounds (VOCs) and greenhouse gases such as carbon dioxide (CO₂) and methane (CH₄) also cause serious health issues [1]. Therefore, there has been an increasing need for a reliable gas sensor to enhance the environment and reduce the spread of harmful gases. Acoustic wave sensors such as surface acoustic wave (SAW) and film bulk acoustic wave resonator (FBAR) are widely employed as sensors, including gas sensors, mass sensors, temperature sensors, and biosensors [2-8]. Due to the interest in developing small-size (µm range) sensors, sensors based on FBAR are extensively researched. Table 1 summarizes the gas sensors' performance using different technologies from previous works. From the table, the findings demonstrate that FBARs function at higher frequencies, typically from sub-GHz to 10 GHz, due to thinner piezoelectric sheets (0.5-3 µm) and a small base mass compared to quartz crystal microbalance (QCM). FBARs have increased sensitivity and sharper resonances because of their high quality(Q)factor, which allows for precise detection of minor frequency shifts. SAW devices, on the other hand, have fundamental frequencies that range from hundreds of MHz to a few GHz, depending on the electrode geometries of the interdigital transducer (IDT). However, SAW efficiency decreases at higher harmonics as compared to FBARs. FBAR provides various advantages, such as small size (µm range), low power consumption, and capability of working at high frequency (GHz range) compared to QCM and SAW sensors [1–2]. Additionally, FBARs can be fabricated using standard MEMS processes such as PiezoMUMPS technology [9]. Therefore, FBAR gas sensors can be produced inexpensively and have the capability to combine multiple sensors on a single chip, integrating them into a single circuit.

FBAR sensor is made up of a thin film of piezoelectric material such as aluminium nitride (AlN) or zinc oxide (ZnO) sandwiched between two metal electrodes such as aluminium (Al), which are top and bottom electrodes, and a sensing layer, polyisobutylene (PIB) as depicted in Figure 1. When an RF signal is applied to the electrodes, the piezoelectric material vibrates at a specific frequency, which is determined by the thickness and properties of the piezoelectric film. Gas sensor based on FBAR operates by measuring the change in resonant frequency of an FBAR resonator when gas molecules adsorb to its surface. Development of gas sensors using FBAR presents a complex challenge centred around the identification of optimal piezoelectric and electrode materials. The resonance frequency, a critical parameter, must be precisely controlled

| Table 1. Summar | v of the gas sensors | application using | g different technologies | [1] | |
|-----------------|----------------------|-------------------|--------------------------|-----|--|
| | | | | | |

| | Quartz Crystal Microbalance (QCM) | Surface Acoustic Wave (SAW) | Film Bulk Acoustic Wave Resonator (FBAR) | |
|--|---|---|---|--|
| Acoustic Wave and Mode | Bulk (shear mode) | Surface (Rayleigh mode) | Bulk (longitudinal mode) | |
| KeyComponents(Materials)Quartz crystalAu electrode | | LiNbO₃, LiTaO₃, ST-Q quartz, La₃Ga₅O₁₄, AlN, GaN and ZnO IDT electrodes | Si, SiO₂, or Si₃N₄ membrane ZnO, AlN and PZT Bottom and top electrode | |
| Detection Principle | The resonance frequency shifts by the adsorption of analytes on the electrode surface | The resonance frequency shifts due to change in electrical properties and viscoelasticity due to the absorbed analytes | The resonance frequency shifts by the adsorption of analytes on the electrode surface | |
| Resonance 5-30 MHz Frequency | | A few MHz – GHz | 100 MHz - 20 GHz | |
| Working Liquids and Gases Medium | | Gases | Liquids and Gases | |
| Sensitivity | Low | Intermediate | High | |
| Pros | Relatively easy to fabricate and use Low cost and high-quality factor Mature technology Detection possible in humid and liquid surrounding High fundamental frequency (HFF) – QCM reported for high sensitivity | Low power consumption Widely used transducer for gas sensor Good sensitivity with large dynamic range, low hysteresis and good linearity Suitable for ppm and ppb concentration Multi layered SAW device for better sensing | Ability to fabricate using standard CMOS technology Detection possible in humid and liquid surrounding Highest quality factor Lowest size approximately 1 × 1 mm³ | |
| Cons | Low detection resolution A thick substrate and large-sized device, which is difficult to scale down | Excessive damping in liquid medium. High wave attenuation in humid condition. | Commercial production of FBAR sensors is uncommon Expensive techniques required Fragile structures and sensitive to many other external parameters | |

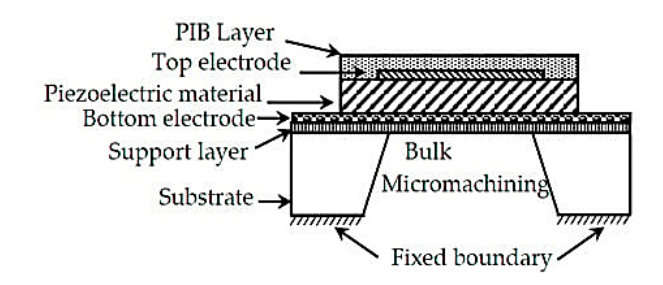


Figure 1. Configuration of FBAR sensor [7]

to ensure efficient vibration, especially in the presence of specific gases that may alter this frequency. Balancing the quality (Q) factor is important, as a higher Q factor contributes to sharper resonances, enhancing sensitivity.

FBAR sensor performance is significantly influenced by the sensing layer, which interacts with target gases, causing measurable resonance shifts and improving sensitivity and specificity [9–10]. The uniformity of this layer is critical for sensor reliability. For gas selectivity, polymer layers like polyimide act as acoustic isolation layers, confining waves within the piezoelectric material and preventing signal loss. A thickness of $\sim\!\!9~\mu m$ optimizes isolation and sensitivity, balancing wave confinement without excessive damping

[10]. Table 2 summarizes the comparison of FBAR gas sensors from different studies. The sensing layer is a crucial component of an FBAR gas sensor, determining its sensitivity, selectivity, and response time.

The choice of sensing layer material and functionalization strategy significantly impacts the sensor's performance. Research is actively exploring new materials and techniques to improve the performance of FBAR gas sensors, such as hybrid materials, bio-inspired materials, and nanocomposites. A PIB layer was an example of the gassensing layer. The PIB polymer is a suitable polymer for gas detection since it has high selectivity to gases and is penetrable; it allows quicker adsorption and desorption and reversibility of the post-vapor analysis exposure, which creates the ideal conditions for gas sensors [7]. Sensitivity itself, a key metric in gas sensing applications, is influenced by the careful selection of materials. Moreover, ensuring material compatibility and stability over time is crucial, as interactions with gases can alter properties. Therefore, this work focuses on enhancing the performance of FBARs in terms of the Q factor to improve the performance of gas sensors. These enhancements involve varying the piezoelectric materials and geometrical parameters of the FBAR at working frequencies of 1 GHz to 6 GHz.

| Ref. | Piezoelectric Material | Piezoelectric Thickness | Electrode Material | k_{eff}^2 | Q factor | Sensitivity | Working Frequency | Detected Gas |
|------|---------------------------|----------------------------|-----------------------------------|-------------|-------------|-------------------------|---|---|
| [9] | ZnO | 4.4 μm | Al 0.2 μm / 0.2 μm | 0.0643 | 1339 | 18908586030 Hz.cm²/g | 472.65 MHz | Acetone |
| [10] | AlN | 1 μm | Al, Pt | - | - | 2.5 Hz/ppm | 1.207 GHz | Chloroform (VOC) |
| [11] | ZnO | 2 μm | Al | - | >1400 | 85.45 Hz/ppm | 1.25 GHz | Volatile Organic Compounds (VOCs) |
| [3] | AlN | 0.5 μm | (Al, Cr) / SOI 1 μm / 10 μm | - | 1 | - | 8.955 GHz (Simulated), 9.4524 GHz (Calculated) | Hydrogen Sulphide (H ₂ S) |
| [12] | ZnO | 1.16 µm | Au 100 nm / 100 nm | - | 750 | - | 1.77 GHz | Methanol, Ethanol, Pentanol, Acetone, Tetrahydrofuran |

Table 2. Comparison of FBAR gas sensors

2. METHODOLOGY

This section focuses on 1-D modelling of FBAR operating at frequencies from 1 GHz to 6 GHz. Two various types of piezoelectric materials, which are AlN and ZnO, are selected. First, the thickness of the piezoelectric layer for each resonance frequency is determined by using Equation (1), where $f_{\text{\tiny S}}$ is the resonance frequency of the FBAR operating in the fundamental longitudinal mode, $\upsilon_{\text{\tiny L}}$ is the acoustic velocity in the longitudinal direction, and t is the thickness of the piezoelectric layer.

$$f = v_L/2t \tag{1}$$

The Mason model is applied in obtaining the electrical input impedance. The electrical input impedance, Z_{in} of a single piezoelectric layer is given in Equation (2) where C_0 is the static capacitance, k^2_{eff} is the mechanical coupling coefficient, $k=\omega/v_L$ (k is the number of waves, ω is angular frequency and v_L is the acoustic velocity) and d is the thickness of piezoelectric layer.

$$Z_{in} = \frac{1}{j_W C_0} \left(1 - k_{eff}^2 \frac{\tan(kd/2)}{kd/2} \right) \tag{2}$$

 C_0 is determined by using Equation (3) where ϵ^s is the permittivity of the piezoelectric layer, d is the thickness of the piezoelectric layer and A is the area. In this work, the area is set to $30 \times 30 \ \mu m^2$, $35 \times 35 \ \mu m^2$ and $40 \times 40 \ \mu m^2$.

$$C_0 = \frac{\varepsilon^{S}A}{d} \tag{3}$$

Meanwhile k^2 eff is calculated by using Equation (4), where f_s and f_p are the series resonance frequency and parallel resonance frequency respectively [13].

$$k_{eff}^2 = \left(\frac{\pi^2}{4}\right) \left(\frac{f_p - f_s}{f_p}\right) \tag{4}$$

Then, Q factors, defined as series resonance frequency, Q_s and parallel resonance frequency Q_p can be obtained by using Equation (5) where Z_{in} is the electrical input impedance and f_s and f_p are the series resonance frequency and parallel resonance frequency, respectively.

$$Q_{s/p} = \frac{f_{s/p}}{2} \left[\frac{d Z_{in}}{df} \right]_{f_s/f_p} \tag{5}$$

In this work, the top and bottom electrodes are fixed to Al. The electrode thickness is set at an optimum ratio of 0.10, representing 10% of the thickness of the piezoelectric layer. This specific ratio has demonstrated better performance, as reported in [14, 15]. To determine the effect of electrode layers on the performance of FBAR, Equation (6) is used.

$$Z_{in} = \frac{1}{j\omega C_o} \left(1 - k^2_{eff} \frac{\tan \theta}{\theta} \frac{(Z_T + Z_B)\cos^2 \theta + j\sin 2\theta}{(Z_T + Z_B)\cos^2 \theta + j(Z_T + Z_B + 1)\sin 2\theta} \right)$$
 (6)

where Z_{ln} is the electrical input impedance, Z_T (top electrode impedance) and Z_B (bottom electrode impedance) are standardized values at the borders of the piezoelectric layer for acoustic impedance and a piezoelectric plate's half phase known as θ is given by $\theta = k/t$ where $k = \omega/v_L$ [14]. The acoustic impedance matching between the two medium determines the piezoelectric layer-to-electrode interface boundary impedances Z_T and Z_B . The values of Z_T and Z_B can be calculated as follows:

$$Z_{T/B} = Z_0^{T/B} \left(\frac{Z_{LOAD} \cos \theta_{T/B} + j Z_0^{T/B} \sin \theta_{T/B}}{Z_0^{T/B} \cos \theta_{T/B} + j Z_{LOAD} \sin \theta_{T/B}} \right)$$
(7)

The top (T) or bottom(B) electrode layers have a characteristic acoustic impedance of $Z_0^{\ T/B}$, where Z_0 is given as:

$$Z_0 = A\rho v_L \tag{8}$$

where area (A), density (ρ), and longitudinal acoustic wave velocity (v_L) are all expressed in these terms. Input load impedance Z_{LOAD} and acoustic-wave phase $\theta_{T/B}$ are two parameters that may be used to describe the acoustic-wave phase across the two electrode layers.

The FBAR detects frequency variations with high precision, enabling accurate identification of mass changes. It is commonly known that adding more mass to the FBAR device's surface reduces the resonance frequency. Therefore, the relationship between the frequency shift and the additional mass can be described by the following

Equation (9) [4]:

$$\Delta f = \frac{2f_o^2}{\sqrt{\mu p}} * \frac{\Delta m}{A} \tag{9}$$

where Δf = frequency change, f_o = resonant frequency, Δm = mass change, μ = elastic constant of the piezoelectric material (g cm⁻¹ s⁻¹), p = density of the piezoelectric material (g/cm³), A = piezoelectrically active area (cm²). This formula was created to track how the increased mass applied to the FBAR device's surface affects the piezoelectric material's resonance frequency. The deposited mass functions as an extension of the thickness of the piezoelectric material on the FBAR device's surface. The relationship between change of frequency and change of mass is that the value of mass sensitivity can be determined by finding the slope of mass change vs frequency change graph by using Equation (10) [2].

$$s_m = \frac{\Delta f}{\Delta m} \tag{10}$$

where s_m = sensitivity mass.

3. RESULTS AND DISCUSSIONS

3.1. Effect of Various Piezoelectric Materials on Resonance Frequencies

Figure 2 shows the effect of various piezoelectric materials on resonance frequencies of AlN and ZnO. It is observed that the resonance frequency increases when the thickness of the piezoelectric material decreases, thus agreeable with Equation (1). It is also observed that the thickness of AlN is thicker than ZnO at the specific resonance frequencies. For example, at the frequency of 6 GHz, the thickness of AlN is 0.87 μ m, meanwhile the thickness of ZnO is 0.53 μ m. This is due to the value of the acoustic velocity for AlN higher than ZnO, which are10400 m/s and 6330 m/s respectively [14].

3.2. Effect of Various Area Size on Static Capacitance (C_0)

In this work, the area size is set to 30 μ m × 30 μ m, 35 μ m × 35 μ m and 40 μ m × 40 μ m. The static capacitance is

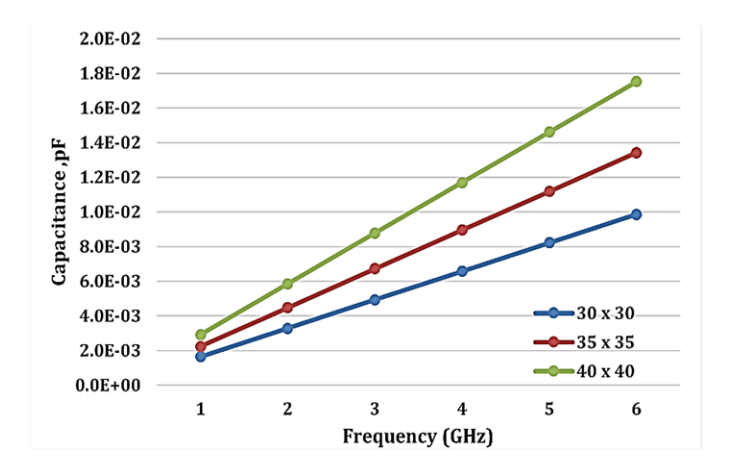


Figure 3. Influence of resonance area on static capacitance using AIN

determined by using Equation (3). The material properties of AlN and ZnO used are as in previous work [14]. Figures 3 and 4 show the effect of various area size on the static capacitance by using AlN and ZnO respectively. From the figures, it is seen that as the resonance area increases, the static capacitance also increases. It is also observed that the values of C_0 for FBAR using ZnO are higher than for FBAR using AlN. The possible reason for this is ZnO has lower permittivity, which is 9.2 compared to AlN, 9.5.

3.3. Effect of Various Area Size on Electrical Input Impedance (Z_{in})

Figures 5 and 6 depict the effect of various area sizes on the electrical input impedance for FBAR using AlN and ZnO at 6 GHz, respectively. The electrical input impedance is calculated by using Equation (2). As can be seen from the graphs, the impedance decreases as the area size increases. The Z_{in} is slightly lower for FBAR using ZnO due to its higher static capacitance.

3.4. Effect of Various Area Size on Quality (Q) Factor

The Q factor values are determined using Equation (5). Table 3 presents the influence of varying area sizes on the

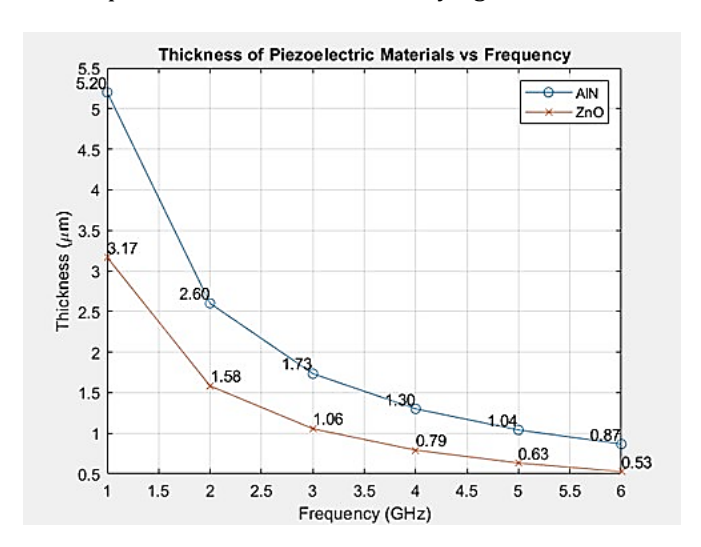


Figure 2. Effect of various piezoelectric materials on resonance frequencies

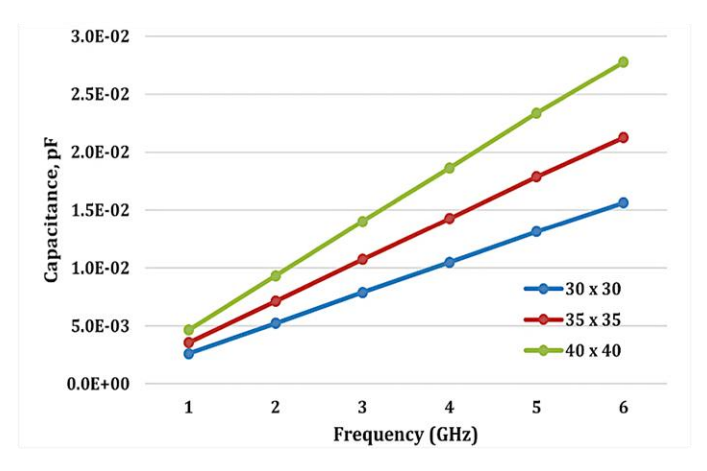


Figure 4. Influence of resonance area on static capacitance using ZnO

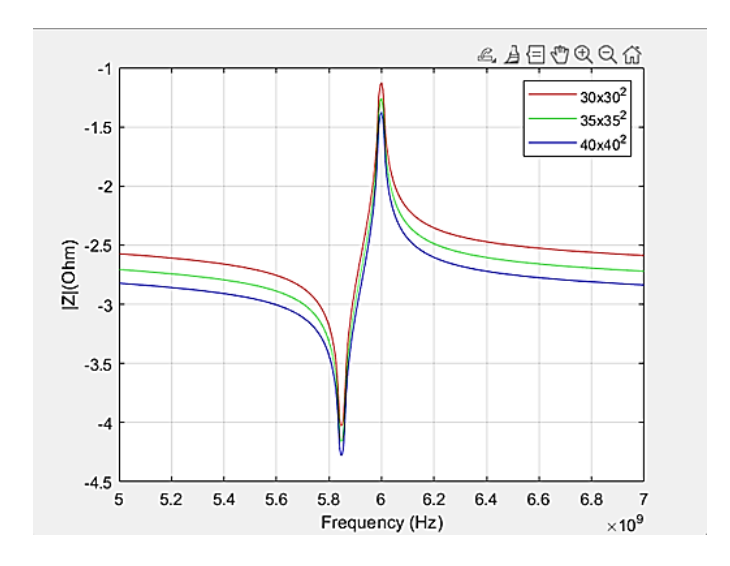


Figure 5. Influence of resonance area on Zin using AlN

Q factor for FBARs employing AlN and ZnO. The results indicate that the Q factor exhibits a decreasing trend with increasing area size. A similar decline in Q factor is also observed with increasing resonance frequency. As shown in the table, the maximum Q factor obtained is 8569 at 1 GHz for the AlN-based FBAR, whereas the ZnO-based FBAR records a maximum Q factor of 3598 at 1 GHz. This enhancement in the AlN-based device can be primarily attributed to the superior intrinsic material properties of AlN compared to ZnO.

3.5. Effect of Top and Bottom Electrode Materials on Resonance Frequency

The analysis is conducted using Equation (6), with the load impedance (Z_{load}) set to 50 Ω . The area size is defined as 25 μ m \times 25 μ m for the top electrode, 30 μ m \times 30 μ m for the piezoelectric layer, and 35 μ m \times 35 μ m for the bottom electrode. Table 4 summarizes the effect of the top and bottom electrodes on the resonance frequency of FBARs utilizing AlN and ZnO. As shown in the table, the resonance frequency decreases with the inclusion of the top and bottom electrode layers. This phenomenon, known as the mass loading effect, occurs when the electrode layers add mass to the resonator structure. The additional mass increases the overall inertia of the device, thereby reducing the resonance frequency. The relationship between mass and resonance frequency is inversely proportional; as the mass increases, the resonance frequency decreases [16].

4. CONCLUSION

A comprehensive analysis of the 1-D modelling of FBAR for gas sensing applications at working frequencies of 1 GHz to 6 GHz has been carried out successfully. The analysis proved that parameters such as the thickness of the piezoelectric layer and the electrode dimensions significantly influence the resonance frequency, static capacitance, and quality factor of the FBAR. Based on the result, employing AlN in FBAR results in the highest Q factor, ranging from 812 to 8569, while maintaining a relatively compact area (30 $\mu m \times 30~\mu m$) and thickness

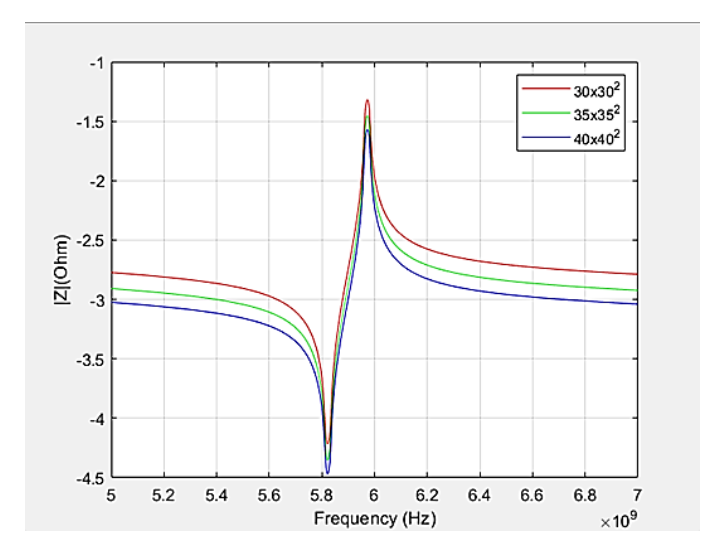


Figure 6. Influence of resonance area on Zin using ZnO

Table 3. Summary of the effect of various area sizes on the Q factors

| Piezoelectric Material | Area | AlN | ZnO |
|-----------------------------|---------|----------|----------|
| Frequency (GHz) / Parameter | (μm²) | Q factor | Q factor |
| | 30 × 30 | 8569 | 3598 |
| 1 | 35 × 35 | 8431 | 2667 |
| | 40 × 40 | 8220 | 2060 |
| | 30 × 30 | 7563 | 2995 |
| 2 | 35 × 35 | 6035 | 2199 |
| | 40 × 40 | 4852 | 1687 |
| | 30 × 30 | 3611 | 1937 |
| 3 | 35 × 35 | 3845 | 1431 |
| | 40 × 40 | 3998 | 1098 |
| | 30 × 30 | 2689 | 1800 |
| 4 | 35 × 35 | 1977 | 1318 |
| | 40 × 40 | 1517 | 1009 |
| | 30 × 30 | 2683 | 1730 |
| 5 | 35 × 35 | 1976 | 1429 |
| | 40 × 40 | 1513 | 1173 |
| | 30 × 30 | 1441 | 1723 |
| 6 | 35 × 35 | 1060 | 1273 |
| | 40 × 40 | 812 | 973 |

Table 4. Summary of top and bottom electrode materials on resonance frequency

| Piezoelectric Material | AIN | | ZnO | |
|-----------------------------------|----------------|-------|------|-------|
| Frequency (GHz) / Parameter | $\mathbf{f_s}$ | f_p | fs | f_p |
| 1 | 0.87 | 0.92 | 0.82 | 0.87 |
| 2 | 1.78 | 1.83 | 1.75 | 1.81 |
| 3 | 2.81 | 2.85 | 2.78 | 2.82 |
| 4 | 3.85 | 3.91 | 3.76 | 3.80 |
| 5 | 4.81 | 4.86 | 4.75 | 4.80 |
| 6 | 5.89 | 6.01 | 5.76 | 5.81 |

(867nm to 5200 nm). It is also shown that the resonance frequency decreases in the presence of the top electrode and bottom electrode. Therefore, the selection of piezoelectric materials and geometrical parameters can be tailored to the specific requirements of the applications. While this work successfully met its objectives, several areas require further research and development to enhance the performance and applicability of FBAR-based gas sensors. Further exploration of advanced materials for the laver and electrodes piezoelectric could improvements in sensor sensitivity and stability. This includes studying the effects of humidity, temperature variations, and prolonged exposure to target gases on sensor performance. Conducting real-world testing and validation of FBAR gas sensors in various environments will provide valuable data for refining sensor designs and improving their robustness and reliability. By addressing these areas, future research can build on the findings of this project, leading to the development of highly efficient, reliable, and cost-effective FBAR-based gas sensors for a wide range of applications.

REFERENCES

- [1] A. Kumar and R. Prajesh, "The potential of acoustic wave devices for gas sensing applications," *Sensors and Actuators A: Physical*, vol. 339, p. 113498, Jun. 2022, doi: 10.1016/j.sna.2022.113498.
- [2] Z. Sabani, A. A. M. Ralib, J. Karim, N. B. Saidin, and N. F. B. M. Razali, "Design and simulation of Film Bulk Acoustic Wave Resonator (FBAR) Gas Sensor Based on ZnO Thin Film," in 2019 IEEE Regional Symposium on Micro and Nanoelectronics (RSM), IEEE, Aug. 2019, pp. 34–37. doi: 10.1109/RSM46715.2019.8943566.
- [3] J. Ren, H. Chu, Y. Bai, R. Wang, P. Chen, and J. Chen, "Research and Design of High Sensitivity FBAR Micromass Sensors," *IOP Conference Series: Earth and Environmental Science*, vol. 632, no. 4, p. 042014, Jan. 2021, doi: 10.1088/1755-1315/632/4/042014.
- [4] Y. Zhang, J. Luo, A. J. Flewitt, Z. Cai, and X. Zhao, "Film bulk acoustic resonators (FBARs) as biosensors: A review," *Biosensors and Bioelectronics*, vol. 116, pp. 1–15, Sep. 2018, doi: 10.1016/j.bios.2018.05.028.
- [5] X. Zhao, Z. Zhao, B. Wang, Z. Qian, and T. Ma, "The Design of a Frame-Like ZnO FBAR Sensor for Achieving Uniform Mass Sensitivity Distributions," *Sensors*, vol. 20, no. 8, p. 2408, Apr. 2020, doi: 10.3390/s20082408.
- [6] A. Kittmann *et al.*, "Sensitivity and noise analysis of SAW magnetic field sensors with varied magnetostrictive layer thicknesses," *Sensors and Actuators A: Physical*, vol. 311, p. 111998, Aug. 2020, doi: 10.1016/j.sna.2020.111998.

- [7] B. Panchal, A. Bhadauria, and S. Varghese, "3D FEM Simulation and Analysis of Fractal Electrode-Based FBAR Resonator for Tetrachloroethene (PCE) Gas Detection," *Fractal and Fractional*, vol. 6, no. 9, p. 491, Sep. 2022, doi: 10.3390/fractalfract6090491.
- [8] S. S. Ba Hashwan *et al.*, "Analytical Modeling of AIN-Based Film Bulk Acoustic Wave Resonator for Hydrogen sulfide Gas detection Based on PiezoMUMPs," *Journal of Physics: Conference Series*, vol. 1962, no. 1, p. 012003, Jul. 2021, doi: 10.1088/1742-6596/1962/1/012003.
- [9] G. Niro, I. Marasco, F. Rizzi, A. D'Orazio, M. Grande, and M. de Vittorio, "Design and Fabrication of a Flexible Gravimetric Sensor Based on a Thin-Film Bulk Acoustic Wave Resonator," *Sensors*, vol. 23, no. 3, p. 1655, Feb. 2023, doi: 10.3390/s23031655.
- [10] I. Marasco, G. Niro, G. Magno, G. Grande, F. Rizzi, and M. de Vittorio, "Innovative-shaped FBARs for smart sensors," in 2023 IEEE Conference on Antenna Measurements and Applications (CAMA), IEEE, Nov. 2023, pp. 710–713. doi: 10.1109/CAMA57522.2023. 10352853.
- [11] G. Zeng *et al.*, "Detection and Discrimination of Volatile Organic Compounds using a Single Film Bulk Acoustic Wave Resonator with Temperature Modulation as a Multiparameter Virtual Sensor Array," *ACS Sensors*, vol. 4, no. 6, pp. 1524–1533, Jun. 2019, doi: 10.1021/acssensors.8b01678.
- [12] A. A. Md Ralib and A. S. Syamsil Omar, "AN Investigation of the Sensitivity of Polymer-coated Surface Acoustic Wave-based Gas Sensors in the Detection of Volatile Organic Compounds," *IIUM Engineering Journal*, vol. 22, no. 2, pp. 168–177, Jul. 2021, doi: 10.31436/iiumej.v22i2.1612.
- [13] N. I. M. Nor *et al.*, "The Design and Analysis of High Q Factor Film Bulk Acoustic Wave Resonator for Filter in Super High Frequency," *International Journal of Nanoelectronics and Materials*, vol. 14 (Special Issue), No. December, pp. 79–85, Dec. 2021.
- [14] N. I. M. Nor, "Wide bandwidth film bulk acoustic wave resonator for Ku-band filters," Bundoora, Victoria, 2013.
- [15] N. I.M. Nor, N. Khalid, H. Aris, M. S. Mispan, and N. Aiman Syahmi, "Analysis of Different Piezoelectric Materials on the Film Bulk Acoustic Wave Resonator," *International Journal of Nanoelectronics and Materials (IJNeaM)*, vol. 16 (Special Issue), No. December, pp. 121–130, Dec. 2023, doi: 10.58915/ijneam.v16iDECEMBER.398.
- [16] Y. Liu, Y. Cai, Y. Zhang, A. Tovstopyat, S. Liu, and C. Sun, "Materials, Design, and Characteristics of Bulk Acoustic Wave Resonator: A Review," *Micromachines*, vol. 11, no. 7, p. 630, Jun. 2020, doi: 10.3390/mi11070630.